JOURNAL OF SOLID STATE CHEMISTRY 110, 167–175 (1994)

Two Structures of $Ag_{2-x}V_4O_{11}$, Determined by High Resolution Electron Microscopy

H. W. Zandbergen,* A. M. Crespi,† P. M. Skarstad,† and J. F. Vente‡

*National Centre for HREM, Laboratory of Materials Science, Delft University of Technology, Rotterdamseweg 137, 2628 AL Delft, The Netherlands; †Medtronic, Inc., 6700 Shingle Creek Parkway, Minneapolis, Minnesota 55430; ‡Gorlaeus Laboratories, University of Leiden, P.O. Box 9502, 2300 RA Leiden, The Netherlands

Received March 23, 1993; in revised form August 19, 1993; accepted August 23, 1993

High resolution electron microscopy and X-ray powder diffraction have been applied to determine the structure and microstructure of $Ag_{2-x}V_4O_{11}$. This compound adopts two structures. Both structures consist of V_4O_{11} slabs, but they differ in the way these slabs are stacked. One stacking leads to a *C*-centered monoclinic unit cell ($C2/m$) with dimensions $a = 1.451(1)$, $b = 0.35766(3)$, $c = 0.9564(8)$ nm, $\beta = 128.74(1)°$ (Phase I) which is dominant and the other stacking to a *C*-centered monoclinic unit cell with dimensions $a = 1.53$, $b = 0.360$, $c = 0.76$ nm, $\beta = 102°$ (Phase II). Ion milling leads to a change in the c axis and β, which is suggested to be caused by a loss of Ag. Frequent stacking defects occur in the c^* direction due to switching from the Phase I to the Phase II structure and due to (001) twinning.

INTRODUCTION

Silver vanadium oxide has been reported as a cathode material for lithium batteries (1). Takeuchi *et al.* (2) have reported that the composition is $Ag_2V_4O_{11}$. Recently we have performed a study on the unit cell of this material (3) and found the unit cell to be *C*-centered monoclinic with cell dimensions $a = 1.533(1)$, $b = 0.3587(2)$, $c = 0.9526(9)$ nm, $\beta = 127.9°$. Based on high resolution electron microscopy, a structure for $Ag_2V_4O_{11}$ is proposed. In this paper we report a more detailed analysis of the high resolution electron microscopy data and a refinement of X-ray powder diffraction data. This research is part of a more extensive study, which aims at the determination of the structures of the compounds occurring in the system $Li–Ag_2V_4O_{11}$ to obtain a better understanding of the discharge reactions and the crystal chemistry.

EXPERIMENTAL

Silver vanadium oxide was prepared by solid state reaction of Ag_2O and V_2O_5 in the ratio 1 : 2 at 500°C in oxygen for 6 hr. Electron transparent specimens for electron microscopy were prepared (i) by grinding and dispersing a few droplets of a suspension of the ground material in ethanol on a carbon coated holey film supported by a Cu grid or (ii) by ion milling of an approximately 20-μm-thick disk, obtained by pressing some ground material with a pressure of 10^3 kg/cm^2. Electron microscopy was performed with a Philips CM30ST electron microscope operating at 300 kV and equipped with side-entry 25°/25° tilt specimen holder.

$Ag_{2-x}V_4O_{11}$ is rather sensitive to the electron beam, resulting in amorphization. This hampers the determination of the structure. However, because for a structure determination one is only interested in the average structure, the experimental image can be averaged, thus reducing the noise due to the image recording and the partial amorphization. Selected images were digitized with about 50 pixels per nm. These images were noise reduced by averaging each pixel over itself and its eight neighbors. Next, the image was averaged over a number of unit cells.

Image calculations were carried out using a MacTempas software program (4). For the calculations, the following instrument parameters were used: spherical aberration is 1.2 mm, defocus spread is 9 nm, beam convergence is 1.2 mrad, objective aperture size is 6.5 nm^{-1} and instrument vibration is 0.05 nm.

X-ray powder diffraction was performed at room temperature using a Philips PW 1050 X-ray diffractometer using monochromated Cu$K\alpha$ radiation. The data were collected digitally in steps of 0.02° 2θ and 10 sec counting time in the range: $10° \leq 2\theta \leq 90°$. The slit width used was 0.1° 2θ. The X-ray diffraction pattern was analyzed using the method described by Rietveld (5). For this purpose the GSAS (version 6.1) computer program developed by Larson and Von Dreele (6) was used. The unit cell parameters, the atomic fractional coordinates, four isotropic thermal parameters (one overall U_{iso} for all oxygen), six background parameters, four profile coefficients (pseudo-Voigt shape), a zero point correction, and a scale factor were refined. No peaks due to Ag or one of the starting materials could be detected.

0022-4596/94 $6.00

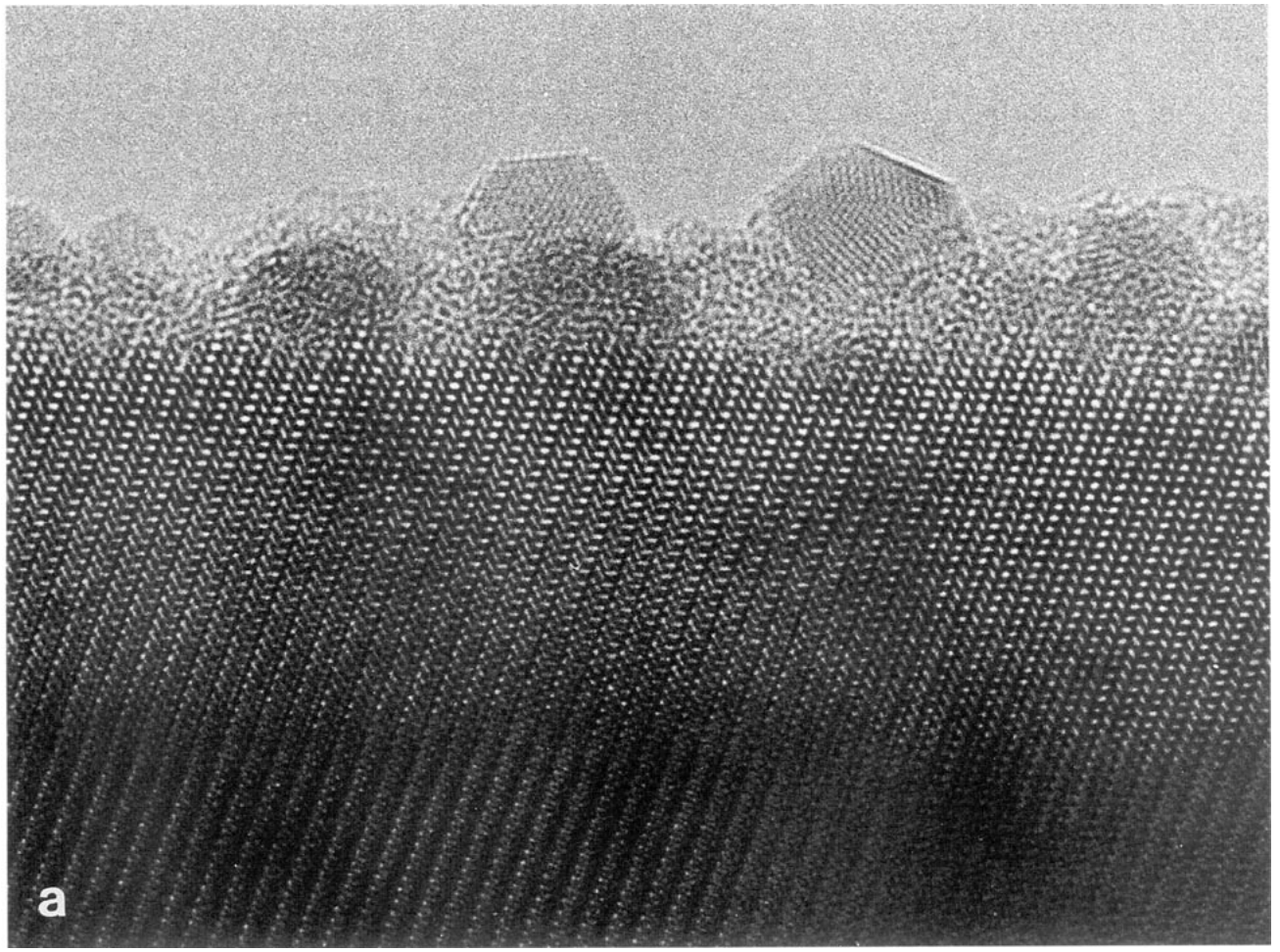

FIG. 1. HREM image of Ag particles on the surface of a $Ag_{2-x}V_4O_{11}$ crystal in [110] orientation. (a) The image taken immediately after orientation of the crystal and (b) taken from the same area after irradiation with the electron beam for 2 min, which resulted in a considerable amorphization. Neither the number of Ag particles nor their size was increased.

EXPERIMENTAL RESULTS

Low resolution transmission electron microscopy shows that $Ag_{2-x}V_4O_{11}$ has a needle-like morphology. Because of this morphology it was not possible to obtain diffraction patterns along the needle direction, because the crystals were too thick in this direction.

By means of electron diffraction the reciprocal space was constructed. This was done by tilting a crystal about a chosen reciprocal lattice vector. With certain tilt intervals electron diffraction patterns were recorded, as well as for intermediate tilts if a symmetric diffraction pattern was obtained. By combination of these electron diffraction patterns and the tilt angles, the reciprocal lattice could be constructed, indicating a *C*-centered monoclinic unit cell with $a = 1.53$, $b = 0.360$, $c = 0.95$ nm, $\beta = 128°$. The electron diffraction experiments on the crushed sample showed the presence of twinning. Rietveld refinement of the X-ray powder diffraction data resulted in the cell dimensions $a = 1.5452(1)$, $b = 0.35766(3)$, $c = 0.9564(8)$ nm, $\beta = 128.744(3)°$.

High resolution electron microscopy was performed on the as-synthesized material with only minor crushing to obtain isolated crystals or small agglomerates of crystals. $Ag_{2-x}V_4O_{11}$ was found to be rather sensitive to the electron beam, resulting in a rapid amorphization when electron doses were used which are normal for recording of high resolution images. All crystal surfaces showed the presence of small Ag particles (see Fig. 1). Longer exposure to the electron beam (see Fig. 1) did not result in the increase of the number of Ag particles or their size. This indicates that the Ag particles are not formed due to the electron beam, but were either already present on the as-prepared material or are formed due to a loss of silver during the sample preparation. The amount of Ag particles was found to vary from crystal to crystal, but all crystal surfaces contained Ag particles, ranging in size from 1 to 5 nm. Figure 1 gives an example of the average Ag loading

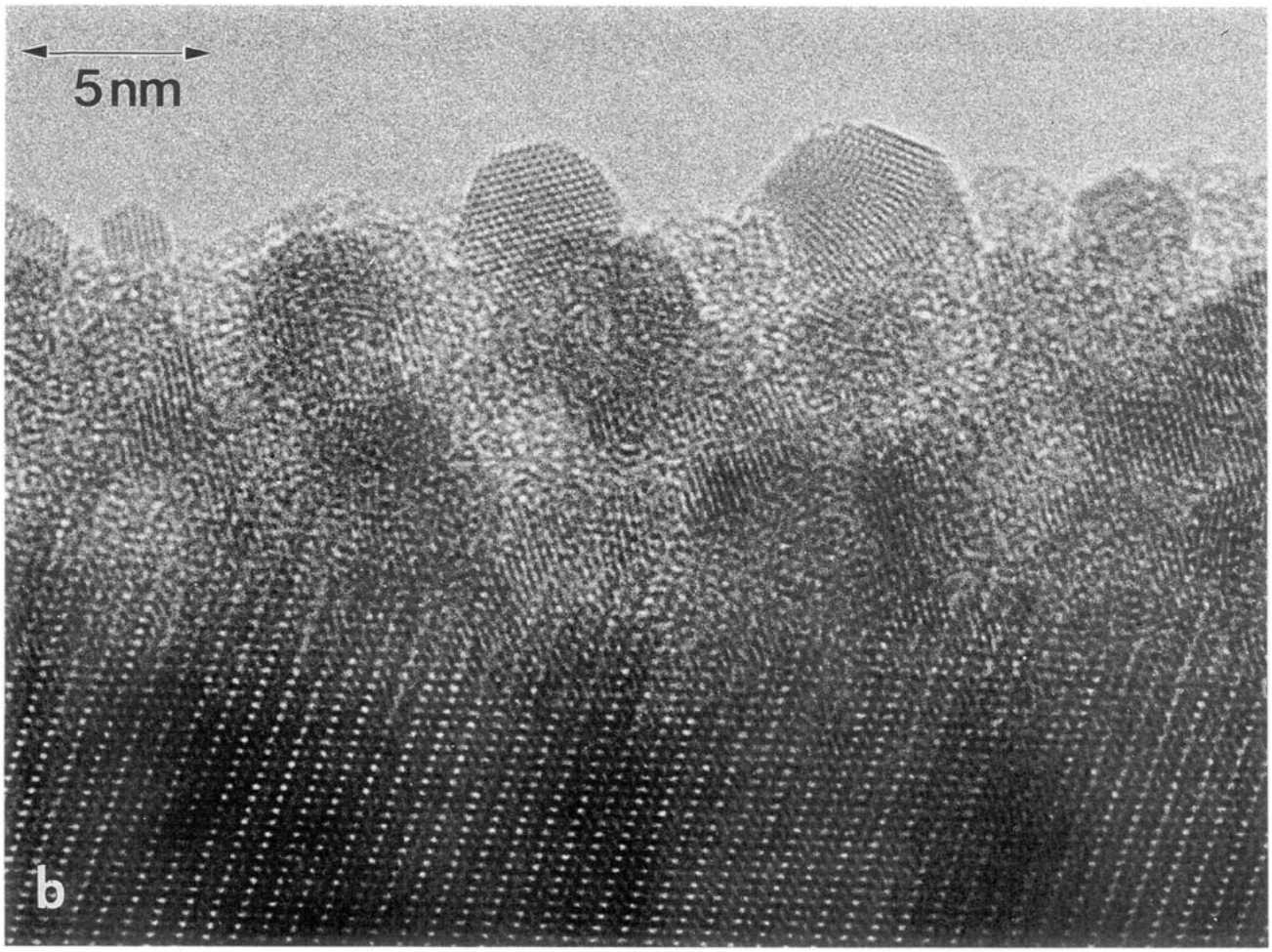

FIG. 1—*Continued*

of the surface. The size and the volume fraction of the Ag particles are so small that they are not revealed by X-ray powder diffraction.

The presence of Ag on the surfaces indicates that the compound may not have the composition $Ag_2V_4O_{11}$ but $Ag_{2-x}V_4O_{11}$. It is difficult to determine the value of x in $Ag_{2-x}V_4O_{11}$ from the volume fraction of the Ag particles on the surface, because the average thickness is difficult to measure and other Ag-rich phases (e.g., Ag or Ag_2O) might be present as well as large particles. A rough estimate assuming an average thickness of the Ag layer on the surface of 2 nm and a particle size of $0.4 \times 0.4 \times 5$ μm gives x as about 0.1. However, refinement of the X-ray data (see below) indicates that the Ag is (almost) fully occupied.

From the electron diffraction experiments it was clear that the best viewing direction to obtain interpretable high resolution images is the [010] direction. In this direction, the unit cell is so short that no or only a few atoms will overlap in projection. Since the b axis coincides with the needle direction, it is rather unlikely that one can obtain by crushing crystal fragments which are sufficiently electron transparent in this direction. Therefore, electron transparent specimens were also prepared by ion milling. This method was found to result in enough thin crystals along [010], but it resulted in an amorphous layer on the specimen surface.

In the ion milled specimens, each crystal contains mainly plate-like Ag particles, which range in size from 5 to 50 nm, and the grain boundaries contain a 10–50-nm-thick layer of Ag (See Fig. 2a). The Ag particles inside the crystal extend far along the a axis, an example of which is given in Fig. 2b. Such kinds of particles were not observed in the specimen obtained by crushing. Investigation of crushed pellets obtained by pressing some ground material with a pressure of 10^3 kg/cm^2 (used as starting material for ion milling) showed the absence of these large Ag particles, and also when the pellet was cooled down to liquid nitrogen temperature. This indicates that the large Ag particles observed in the ion milled specimens are not formed during the preparation of the pellets by pressing with 10^3 kg/cm^2. From these observa-

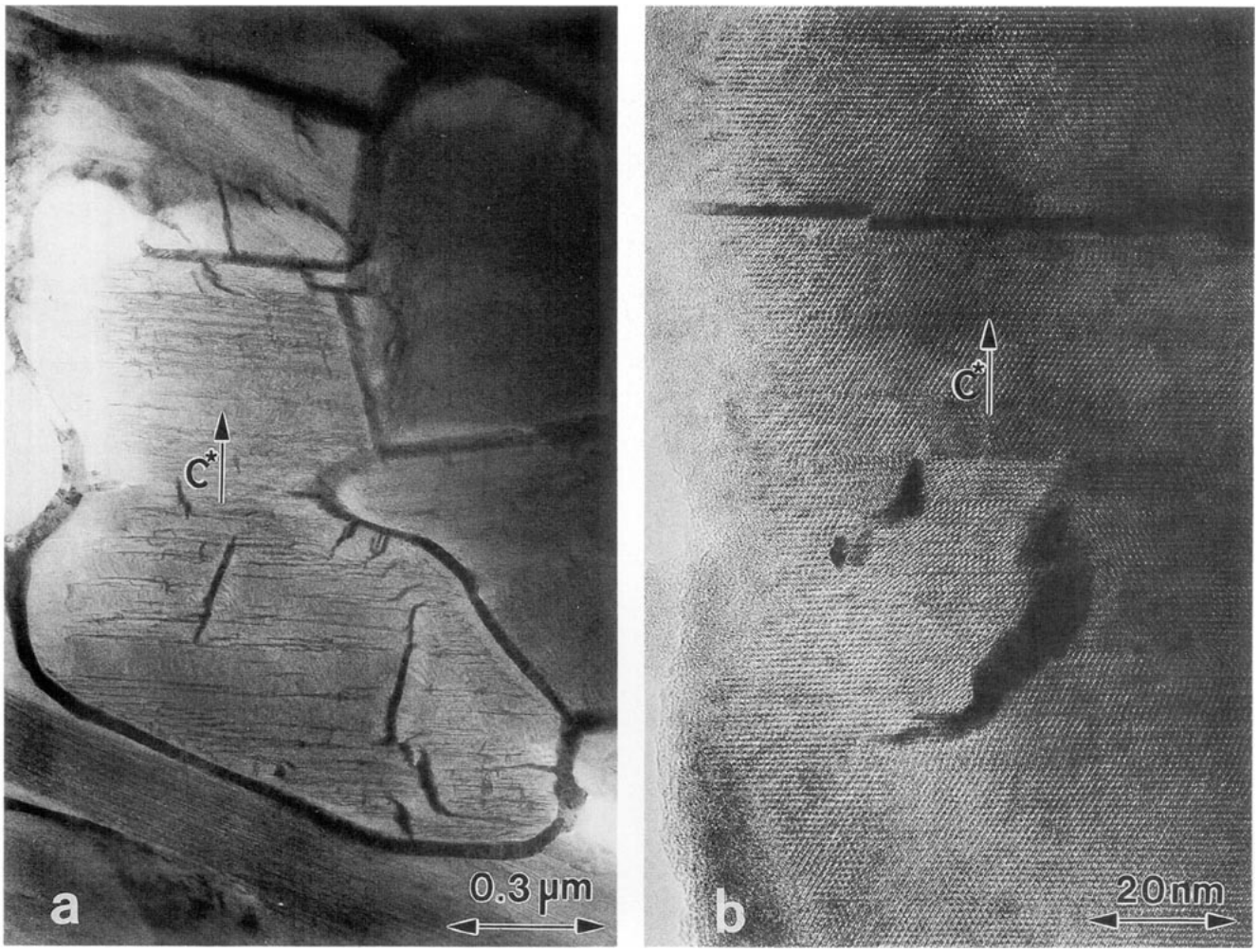

FIG. 2. (a) Low resolution micrograph, showing the presence of a Ag coating of the grain boundaries, and some randomly oriented Ag particles and thin plate-like (001) oriented Ag particles in the grains. (b) [010] HREM image showing the presence of Ag precipitates in a $Ag_{2-x}V_4O_{11}$ crystal.

tions it can be concluded that these Ag particles are formed during the ion milling process. One possible mechanism is the recrystallization of the Ag atoms of the ion sputtered $Ag_{2-x}V_4O_{11}$. A second mechanism involves the recrystallization of Ag obtained by a loss of Ag from the lattice of the $Ag_{2-x}V_4O_{11}$ crystals. The latter mechanism could be caused by the current which passes through the crystals, due to the ion milling processes.

[010] electron diffraction of the ion milled specimen showed that the crystal is not a single crystal but contains a number of defects. Streaking along the c^* direction indicated stacking defects in that direction. The presence of a set of extra reflection spots indicated that the crystal is (001) twinned.

HREM imaging of the [010] oriented crystals from which electron diffraction suggested streaking and twinning showed the presence of planar (001) defects and twinning, whereby the (001) plane is the twin plane. An example is presented in Fig. 3.

The HREM image shown in Fig. 4 shows the existence of two structures. For the first structure, Phase I, being the majority phase, a two-dimensional unit cell $a = 0.77$, $c = 0.90$ nm, $\beta = 125°$ is observed; this would correspond with a C-centered monoclinic unit cell with $a = 1.53$, $b = 0.360$, $c = 0.90$ nm, $\beta = 125°$. Note that the c axis is much smaller than the c axis of the unit cell of the non-ion milled specimen: $c = 0.95$ nm and the difference in β (125° versus 128°). Also a variation of several degrees in β is observed, even in one crystal. The structure image of Phase II deviates from that of Phase I only by a different stacking along the c^* axis. The Phase II structure has a two-dimensional unit cell of $a = 0.77$, $c = 0.72$ nm, $\beta = 102°$. The structural similarities between Phase I and II suggest the unit cell of Phase II to be C-centered monoclinic with $a = 1.53$, $b = 0.36$, $c = 0.72$ nm, $\beta = 102°$. Assuming the same relative decrease in the c axis due to the ion milling procedure as for Phase I, the cell dimensions of the as-synthesized

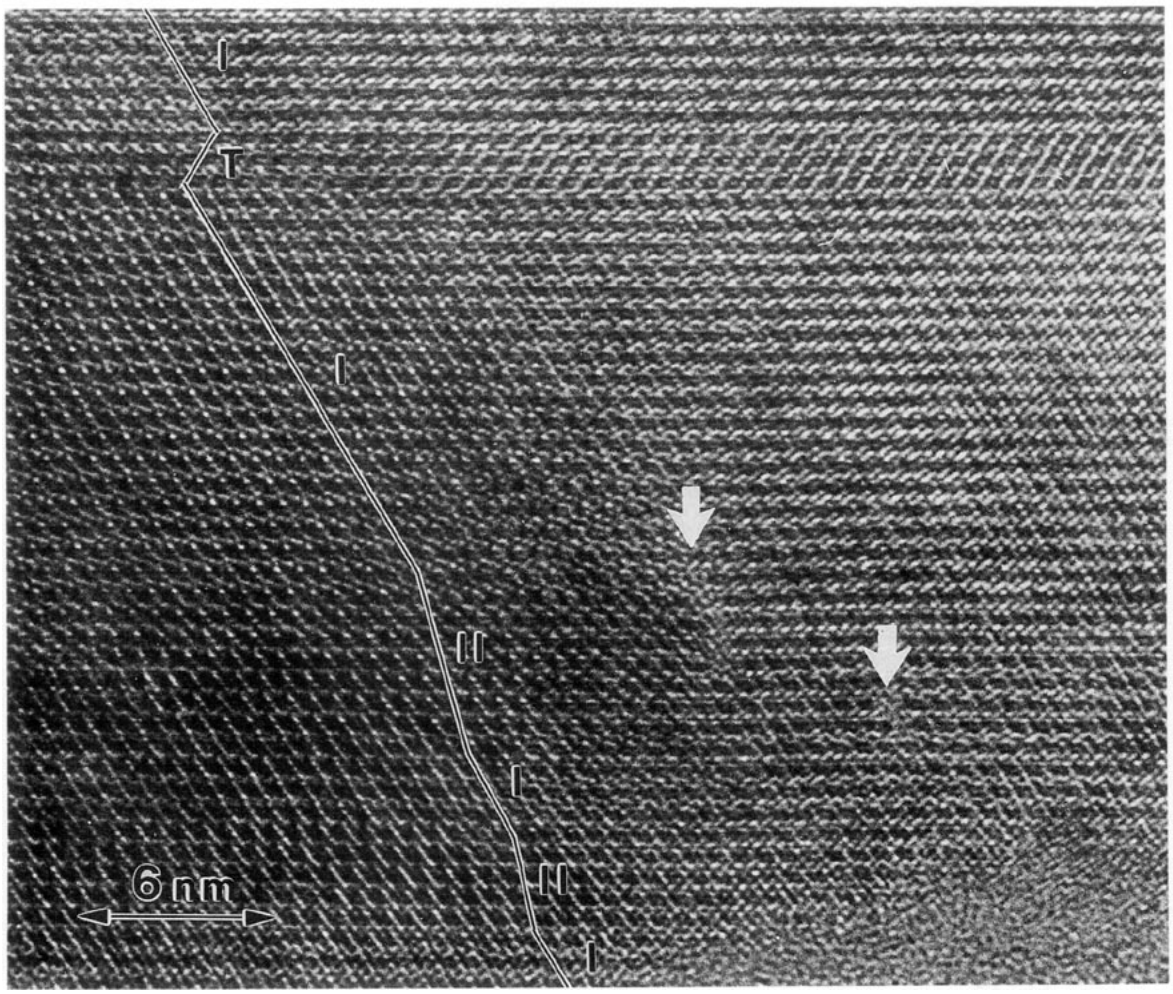

FIG. 3. [010] HREM image of $Ag_{2-x}V_4O_{11}$ showing the presence of stacking defects and (001) twins. The stacking is indicated by a line. Defects occur (indicated by white arrows) when different stackings within one (001) plane meet.

Phase II material would be $a = 1.53$, $b = 0.36$, $c = 0.76$ nm, $\beta = 102°$.

Further enlargements of averaged HREM images of Phase I and Phase II are shown in Fig. 5. The imaging conditions are chosen such that the heavy scattering atoms (the cations) are imaged as black dots. This can be done because (i) the axis in the viewing direction is small (0.36 nm), (ii) the defocus of the microscope can be estimated with an accuracy of less than 10 nm from the image of the amorphous edge of the specimen, and (iii) from the change in image going from the edge to thicker areas one can determine the area in which the phase contrast is dominating. This makes it relatively easy to determine the basic structure for the two phases. Taking into account the structure of a number of vanadates and the composition, one can interpret the groups of four dark dots as groups of four V ions and the two more separated dots as the Ag ions. With this assumption, a structure is obtained for the Phase II which is closely related to that reported for $Cu_{1.8}V_4O_{11}$ (7), whereas the structure for Phase I is one which has not yet been reported for any compound.

The HREM images of Phase I and Phase II are very similar. Both contain slices of groups of four V atoms along the c axis, whereas the Ag atoms are situated between these slices. There are several good reasons to assume that the proposed structures are right: (i) the imaging conditions are chosen such that the cations are imaged as dark dots, thus allowing determination of the positions of these ions, (ii) in many vanadates similar blocks of four V atoms occur (7–10), and (iii) the proposed positions for Phase II are in good agreement with the positions reported for $Cu_{1.8}V_4O_{11}$ (7), which were determined from single crystal X-ray diffraction data.

Image calculations were carried out with a model (see Fig. 6b) for the Phase II structure with the atomic coordinates reported for $Cu_{1.8}V_4O_{11}$ (7), taking into account the reduction of the c axis by assuming rigid V_4O_{11} slabs. A calculated image for a crystal thickness of 3 nm and a

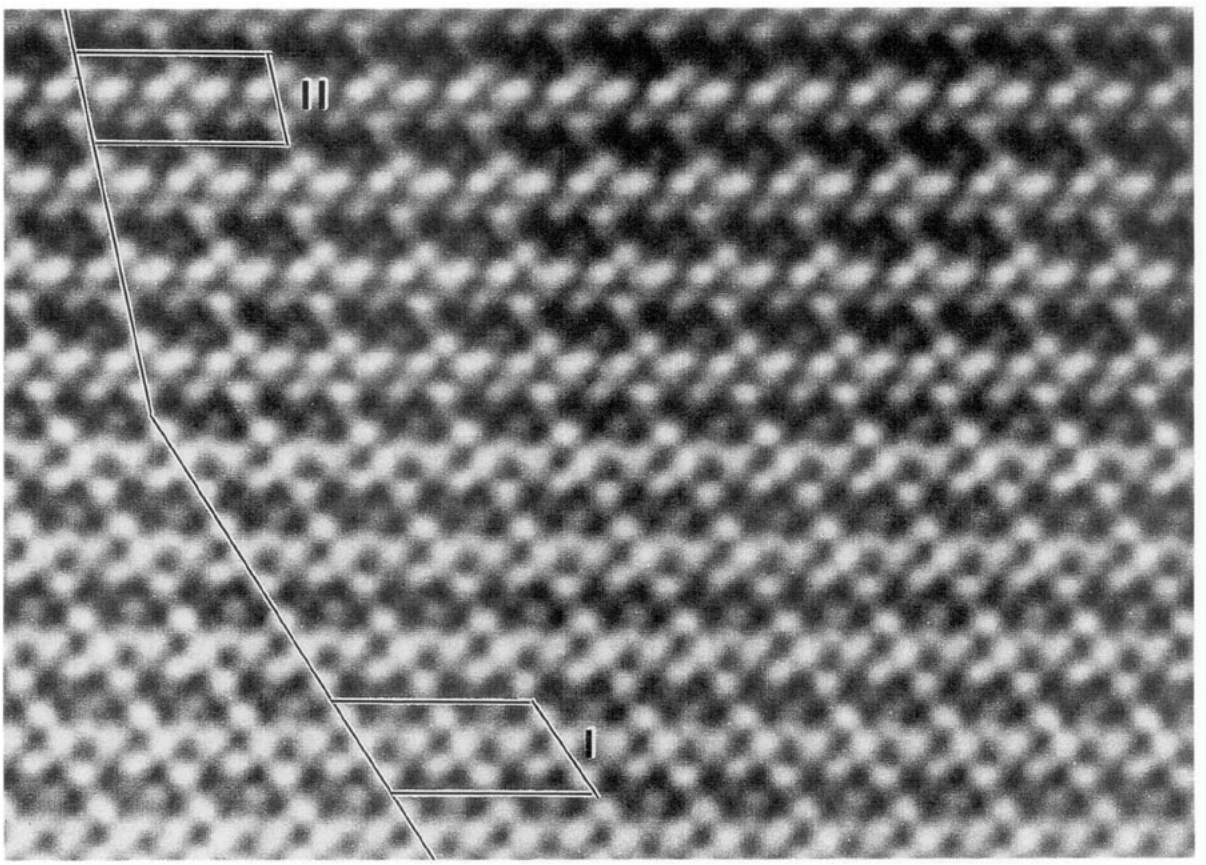

FIG. 4. [010] HREM image, averaged over 16 unit cells along the c axis. Two different structures can be observed: Phase I and Phase II, as is indicated in the text. The unit cells are given as black on white lines.

defocus of −40 nm is given in Fig. 5. A good agreement between the experimental and calculated image is obtained.

Image calculations were also carried out with a model (see Fig. 6a) for the Phase I structure. For this model, rigid V_4O_{11} ribbons occurring in the structure of $Cu_{2-x}V_4O_{11}$ and Phase II $Ag_{2-x}V_4O_{11}$ were shifted with respect to each other such that an angle β of 125° was obtained; the positions of the Ag atoms were determined from the experimental HREM images. This resulted in the monoclinic space group $C2/m$. A good match was obtained between the experimental and calculated images, as can be seen in Fig. 5.

Using this model, a structure refinement in space group $C2/m$ using X-ray powder diffraction data was performed. The refinement converged to a structure very similar to the one suggested by high resolution electron diffraction. Figure 7 shows the agreement between the calculated and measured intensities of $Ag_2V_4O_{11}$. For the final residuals these values were found: R_{wp} = 20.4, R_p = 15.6, DW-d = 0.33, χ^2 (red) = 7.06. The DW-d value is smaller than the lower extreme of the 90% confidence interval; the estimated standard deviations are thus underestimated due to serial correlation (11). The presence of Phase II material is not taken into account in the refinement. Table 1 gives the fractional atomic coordinates and the thermal parameter. Selected atomic distances and angles are given in Table 2. Refinement of the occupancy of Ag (using one overall U_{iso}) resulted in a parameter of 0.96(1), indicating no significant vacancies at this site.

The spots on the Ag sites in the experimental HREM images are less dark than in any of the calculated images of the models with composition $Ag_2V_4O_{11}$, which indicates that the Ag positions are not fully occupied. The actual occupancy was estimated by comparison of the gray values of the Ag and V sites, using line scans in the experimental and calculated images, resulting in occupancies of about 0.9 for both the Phase I and Phase II structures.

DISCUSSION

$Ag_{2-x}V_4O_{11}$ can adopt two crystal structures, as given in Fig. 6. Both structures were determined with HREM. The still unknown structure of Phase I is further refined by a Rietveld refinement of X-ray powder diffraction data. The interatomic distances in the model for Phase I are

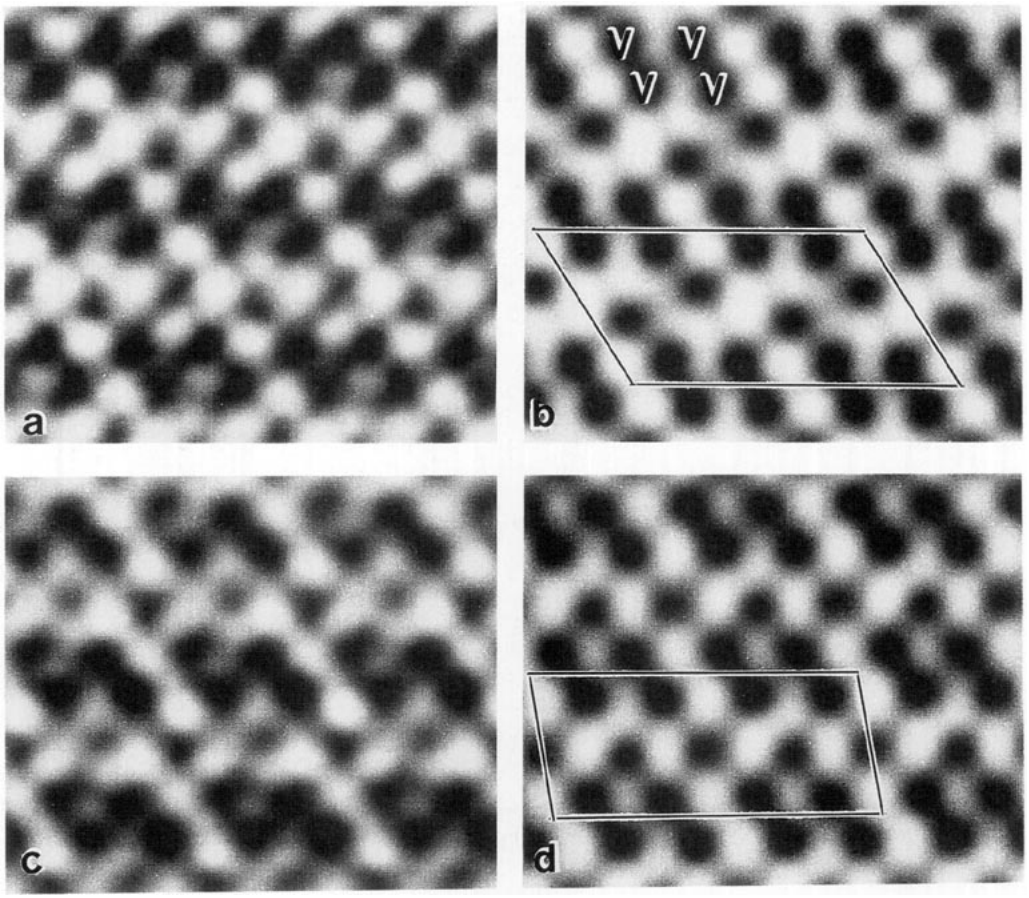

FIG. 5. Experimental and calculated [010] HREM images. (a) An experimental HREM image of Phase I averaged over 16 unit cells along the a axis. (b) The corresponding calculated image. (c) An experimental HREM image of Phase II averaged over 16 unit cells. (d) The corresponding calculated image. A group of four V atoms is indicated in (b). The unit cells are given as black on white lines in (b) and (d).

in good agreement with the Ag–O and V–O distances observed in $Cu_{1.8}V_4O_{11}$ (7) and $Ag_{4-x}V_4O_{12}$ (12). Also the geometry of the oxygen atoms around Ag (5-fold symmetry) and V (distorted octahedron) agrees well with literature. In the X-ray refinement the {002} and {003} reflections show the largest difference between calculated and experimental intensities. The intensity of these reflections as all other {001} reflections are expected to be increased most by the presence of twins and Phase II.

A large difference is observed for the length of the c axis in as-synthesized material and the material prepared by ion milling. Probably the decrease in the c axis is not

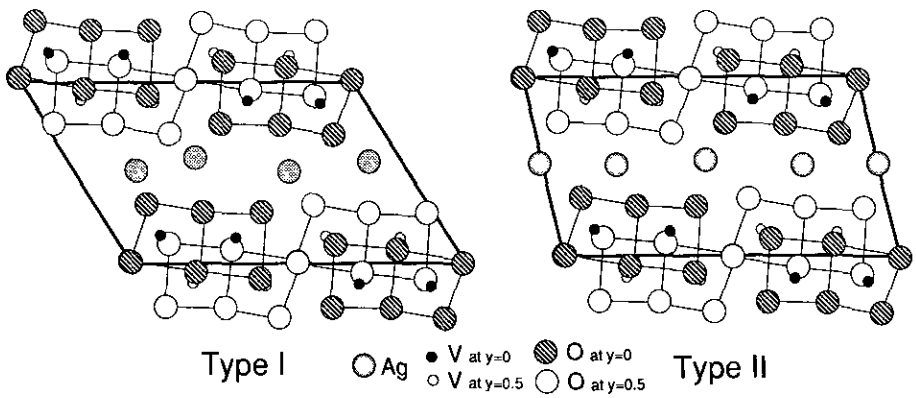

FIG. 6. Schematic representations of the structures for (a) Phase I $Ag_{2-x}V_4O_{11}$ and (b) Phase II $Ag_{2-x}V_4O_{11}$.

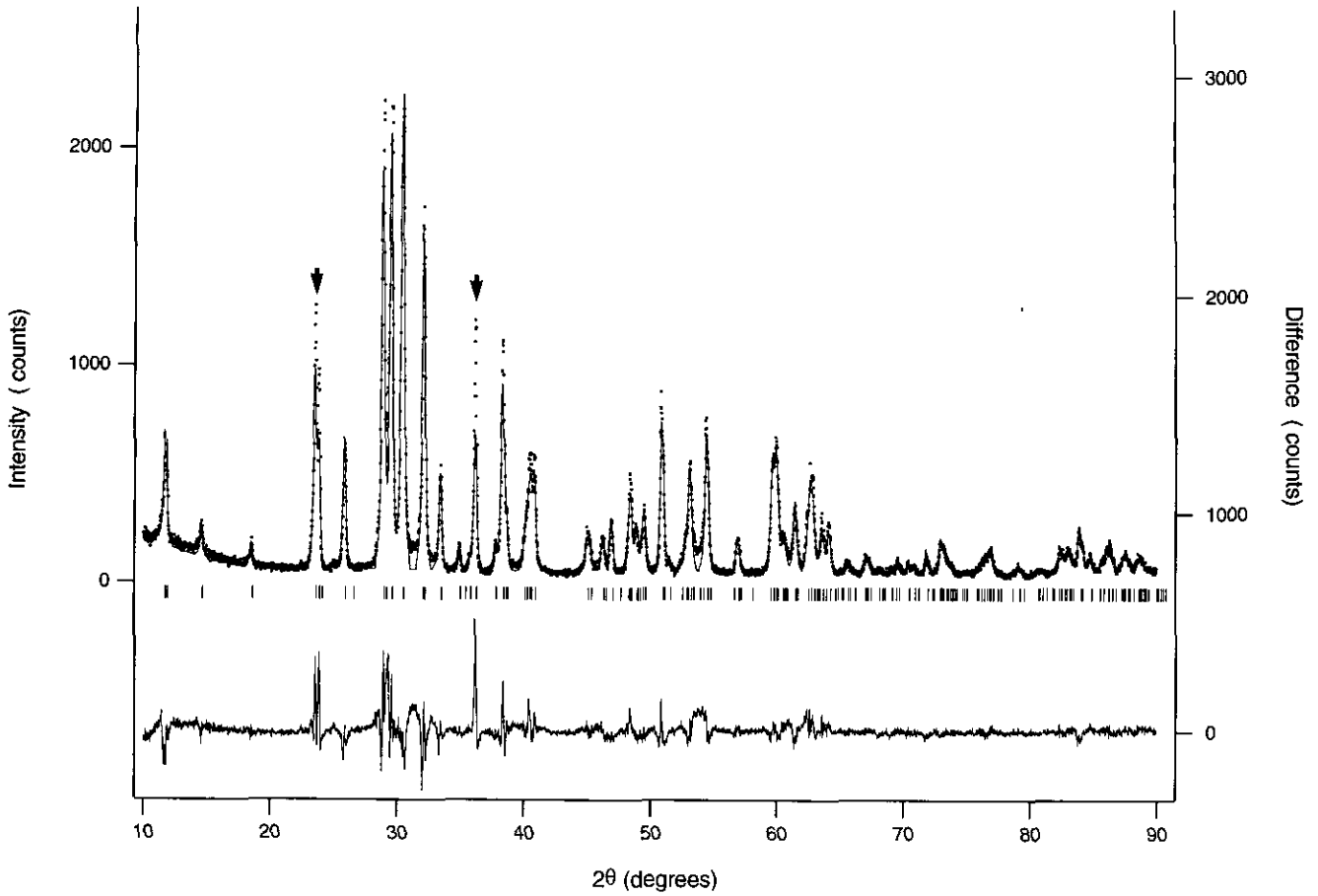

FIG. 7. Observed (dots) and calculated (full line) X-ray diffraction pattern of $Ag_2V_4O_{11}$ at room temperature. The difference ($I_{obs} - I_{calc}$) curve appears at the bottom of the figure. Tick marks below the profile indicate the position of the Bragg reflections included in the calculation. The {002} and {003} reflections are indicated by arrows.

due to compression of the V_4O_{11} slabs but mainly due to the reduction of the distance between the slabs, and possibly also due to some rotation of the V_4O_{11} units in the V_4O_{11} slabs. We suggest that the decrease in the length in the c axis is due to a loss of Ag. This will create space allowing the reduction of the distance between the V_4O_{11} slabs and some rotation of the V_4O_{11} units. This suggestion is in accordance with the presence of Ag precipitates in the $Ag_{2-x}V_4O_{11}$ crystals, as shown in Fig. 3.

The structure model for Phase I, suggested by the HREM images, was found to be easily refined with Rietveld analysis of the X-ray diffraction data. Since the HREM images of both phases are very similar, the X-ray result also indicates that the structure proposed for Phase II $Ag_{2-x}V_4O_{11}$ is right. Moreover, the positions of the Ag and V atoms in Phase II $Ag_{2-x}V_4O_{11}$ determined directly

TABLE 1
Fractional Atomic Coordinates[a] and Thermal Parameters of Phase I $Ag_2V_4O_{11}$

Atom	x	z	U_{iso}[b]
Ag	0.1197(3)	0.5093(6)	0.027(1)
V(1)	0.1469(5)	0.1425(11)	0.017(3)
V(2)	0.3654(6)	0.1472(11)	0.014(2)
O(1)	0	0	0.021(3)
O(2)	0.646(2)	0.088(3)	0.021(3)
O(3)	0.845(2)	0.091(2)	0.021(3)
O(4)	0.188(2)	0.347(3)	0.021(3)
O(5)	0.321(2)	0.273(3)	0.021(3)
O(6)	0.518(2)	0.325(3)	0.021(3)

[a] All atoms at 4(i): x,0,z; except O(1) at 2(a): 0,0,0.
[b] One overall U_{iso} for all O.

TABLE 2
Selected Distances (Å) for Phase I $Ag_2V_4O_{11}$

Ag distances		V(1) distances		V(2) distances	
Ag–O(4)	2.34(2)	V(1)–O(1)	1.77(1)	V(2)–O(2)	2.13(2)
Ag–O(5) 2×	2.44(2)	V(1)–O(2) 2×	1.86(1)	V(2)–O(3)	2.55(2)
Ag–O(6) 2×	2.30(2)	V(1)–O(3)	2.31(2)	V(2)–O(3) 2×	1.84(1)
		V(1)–O(4)	1.63(2)	V(2)–O(5)	1.71(2)
		V(1)–O(5)	2.15(2)	V(2)–O(6)	1.85(2)

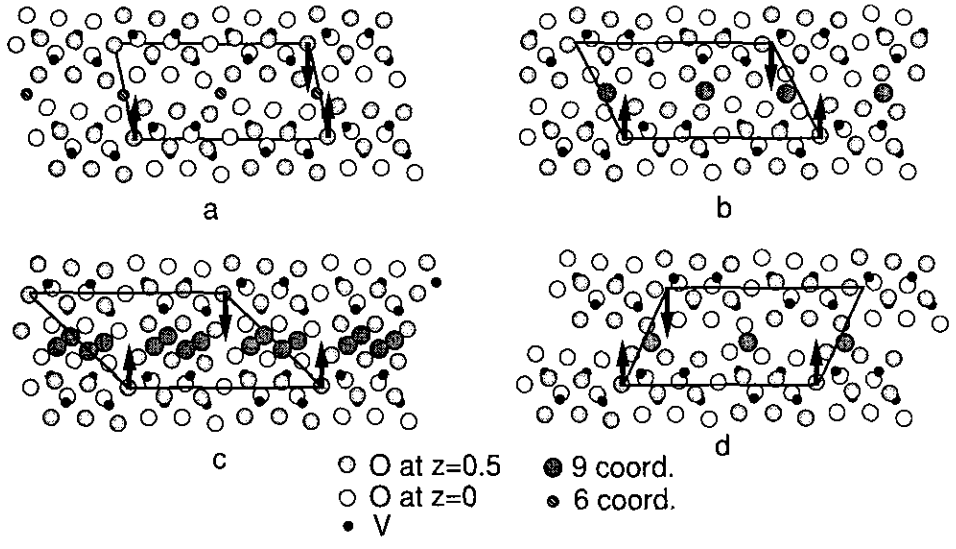

FIG. 8. Schematic representations of the structures which can be obtained by shifting V_4O_{11} along the a axis; (a) and (b) are realized as structures of $Ag_{2-x}V_4O_{11}$; (c) and (d) have not been observed yet.

from the experimental images already fit quite well with the positions of Cu and V atoms reported for $Ag_{2-x}V_4O_{11}$. Also, the V_4O_{11} slabs occur in a rather rigid way as well in a number of vanadates like $Cu_{1.8}V_4O_{11}$ (7), $K_{0.5}V_2O_5$ (8), $Cu_{0.6}V_2O_5$ (9), and $Na_{0.6}V_5O_{15}$ (10).

Phase I and Phase II $Ag_{2-x}V_4O_{11}$ consist of V_4O_{11} slabs along the (001) plane. The V atoms in these slabs have a distorted 6 coordination. Similar slabs and coordinations occur for a number of vanadates. The structures of Phase I and Phase II differ only in the way these slabs are stacked along the c^* direction, as can be seen from Fig. 6. In Phase II $Ag_{2-x}V_4O_{11}$ the Ag ions adopt two positions (see Fig. 6), both with rather irregular oxygen coordination. Phase I $Ag_{2-x}V_4O_{11}$ has only one Ag position, due to the higher symmetry of the structure. The Ag position occurring in Phase I resembles one of the two Ag positions (Cu(1) in $Cu_{1.8}V_4O_{11}$ (7)) in the Phase II structure. The Cu(2) position in $Cu_{1.8}V_4O_{11}$ (7) is only 84% occupied. Possibly the occurrence of both structure types is related to the Ag content, although considering the close resemblance of the two structures, it would not be surprising that both structures are adopted, even if there is no composition difference.

New structures, which are not yet realized, can be constructed by different shifts of neighboring V_4O_{11} slabs. One could move one slab with respect to the other and take those orientations in which well-defined spaces for the additional cations are formed. Several structures are given in Fig. 8. Two of these structure models seem to have even better positions for the large cations like Ag^+ than the observed structures: the models in Figs. 8c and 8d have one and two 9-coordinated positions, respectively, in which the Ag^+ ion would fit nicely. Possibly these structures can be realized if one takes larger cations than Ag^+.

REFERENCES

1. E. S. Takeuchi and P. Piliero, *J. Power Sources* **21,** 133 (1987).
2. E. S. Takeuchi and W. C. Thiebolt, *J. Electrochem. Soc.* **135,** 2691 (1988).
3. A. M. Crespi, P. M. Skarstad, H. W. Zandbergen, and J. Schoonman *in* "Proceedings Symposium on Lithium Batteries." Vol. 93–94, p. 98, The Electrochemical Society, New York, 1993.
4. R. Kilaas and M. A. O'Keefe *in* "Computer Simulation of Electron Microscope Diffraction and Images (W. Krakow and M. O'Keefe, Eds.), p. 171. Minerals Metals, Warrendale, PA, 1989.
5. H. M. Rietveld, *J. Appl. Crystallogr.* **15,** 430 (1982).
6. A. C. Larson and R. B. von Dreele, Generalized Crystal Structure Analysis System (GSAS), Los Alamos Report LAUR 86-748, Los Alamos Natl. Lab.
7. J. Galy and D. Lavaud, *Acta Crystallogr. Sect.* **B27,** 1005 (1971).
8. J. M. Savariault and J. Galy, *J. Solid State Chem.* **101,** 119 (1992).
9. J. Galy, J. Darriet, A. Casalot, and J. B. Goodenough, *J. Solid State Chem.* **1** 339 (1970).
10. A. D. Wadsley, *Acta Crystallogr.* **8,** 695 (1955).
11. R. J. Hill and H. D. Flack, *J. Appl. Crystallogr.* **20,** 356 (1987).
12. Y. N. Drozdov, E. A. Kuzmin, and N. V. Belov, *Sov. Phys. Crystallogr. Engl. Transl.* **19,** 36 (1974).